Diachronous decratonization of the Sino-Korean craton: Geochemistry of mantle xenoliths from North Korea

Jin-Hui Yang[1,2*], Suzanne O'Reilly[2], Richard J. Walker[3], William Griffin[2], Fu-Yuan Wu[1], Ming Zhang[2], and Norman Pearson[2]
[1]State Key Laboratory of Lithospheric Evolution, Institute of Geology and Geophysics, Chinese Academy of Sciences, P.O. Box 9825, Beijing 100029, China
[2]GEMOC ARC Key Centre, Department of Earth and Planetary Sciences, Macquarie University, NSW 2109, Australia
[3]Isotope Geochemistry Laboratory, Department of Geology, University of Maryland, College Park, Maryland 20742, USA

ABSTRACT

Ancient cratons are typically characterized by thick lithospheric-mantle roots that provide them with buoyancy and rigidity. Once formed, cratons, including their roots, move around Earth's surface as parts of rigid plates that are normally unaffected by later magmatism or tectonic activity. Considerable geophysical and geochemical evidence, however, suggests that the ancient lithospheric mantle beneath the Chinese portion of the eastern Sino-Korean craton was replaced by thinner, hotter, juvenile mantle during the Jurassic to Early Cretaceous. The extent and cause of the changes to this lithospheric mantle have been debated. Keys to deciphering the history of the changes include knowledge of both the lateral extent of the lithospheric modifications and the relative timing of change across the craton. Discerning the age and structure of lithospheric mantle underlying North Korea, the easternmost part of the Sino-Korean craton, is thus particularly important. Here we report mineral compositions and Re-Os isotopic data for peridotite xenoliths from North Korean Triassic kimberlite and Tertiary basalts. The data suggest that, from the Triassic to the present, North Korea has been underlain by young, hot and fertile lithospheric mantle, unlike typical cratonic lithospheric roots, but similar to the juvenile lithospheric mantle underlying Chinese portions of the craton. Given the generally ancient nature of the crust composing North Korea, our findings suggest that modification of underlying cratonic roots extended to the eastern edge of the craton. The Triassic eruption age of the kimberlite suggests that the lithospheric changes may have occurred earlier than in China, indicating that lithospheric removal evolved from east to west. These results are most consistent with the conclusion that lithospheric loss was initially triggered by extension that followed the collision between the Sino-Korean and Yangtze cratons.

INTRODUCTION

The Sino-Korean craton, composed of the North China craton and North Korea, is one of the major Archean cratons in eastern Eurasia. It formed and stabilized during Paleoproterozoic time (Zhao et al., 2001), and was subsequently covered by a thick sequence of Proterozoic to Paleozoic sediments (Wang and Mo, 1996). Peridotite xenoliths from Middle Ordovician diamond-bearing kimberlites in China (Fig. 1) provide evidence that ancient (ca. 2.5 Ga), refractory, thick (>~200 km) and cold (geotherm ~40 mW/m^2) lithospheric mantle roots were present beneath at least some parts of the craton prior to Middle Ordovician time (e.g., Menzies et al., 1993; Griffin et al., 1998; Gao et al., 2002; Fan et al., 2000; Xu, 2001). This observation is consistent with the concept that partial melting of the mantle that leads to the creation of continental crust may also produce residual subcontinental lithospheric mantle that is buoyant and rigid, due to its increased Mg# and decreased water contents, relative to ambient convecting upper mantle (Boyd et al., 1997). Consequently, the crust and the lithospheric mantle keel may become mechanically and chemically coupled for billions of years (Walker et al., 1989).

*E-mail: jinhui@mail.igcas.ac.cn.

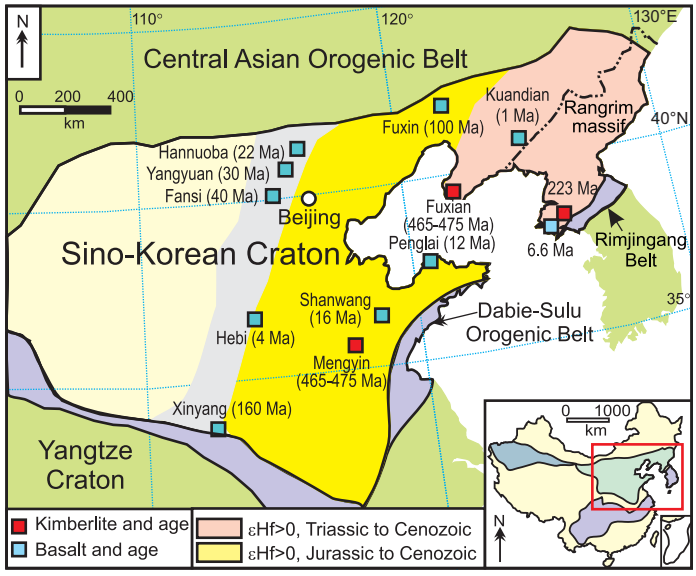

Figure 1. Map showing distribution of xenolith-bearing kimberlites and Mesozoic to Cenozoic alkaline basalts with ages and age distribution of magmas with depleted mantle signatures [$\varepsilon_{Hf}(t) > 0$] in eastern Sino-Korean craton (location in inset). Distributions of magmas with positive $\varepsilon_{Hf}(t)$ are based on data of Yang et al. (2008). Ages of kimberlites from Mengyin and Fuxian in eastern China are 465–475 Ma (Yang et al., 2009), whereas the age of kimberlites from North Korea is ca. 223 Ma. Other age data are from Zheng et al. (2007) and references therein.

In contrast to the state of the lithospheric mantle during the Middle Ordovician, modern geophysical data, as well as the geochemical characteristics of peridotite xenoliths transported by Cenozoic basalts, indicate the current presence of thin, hot, and fertile lithosphere beneath the same area. These observations suggest that the ancient craton has been reactivated, and more than 100 km of cratonic lithosphere has been removed (Menzies et al., 1993; Griffin et al., 1998; Xu, 2001; Wu et al., 2006; Zheng et al., 2007). Although changes in magma compositions can provide some constraints on the timing of lithospheric removal and transformation (Yang et al., 2008), direct evidence of the timing of this process has been scarce, and the resulting uncertainty has influenced debate on the causative mechanisms. Peridotites are the main component of the lithospheric mantle, and because of its utility for constraining the timing of melt removal from peridotites, the Re-Os isotopic system is commonly used for dating the formation of subcontinental lithospheric mantle (e.g., Shirey and Walker, 1998; Alard et al., 2005), and is applied here.

GEOLOGICAL SETTING

North Korea consists of two main tectonic provinces, the Rangrim massif and the Rimjingang belt. The Rimjingang belt is characterized by the occurrence of high-pressure eclogite and gneiss and has been interpreted as the eastward extension of the Qinling-Dabie-Sulu orogenic belt

(Kwon et al., 2009), which formed by the Late Permian to Early Triassic collision between the Sino-Korean and Yangtze cratons. The Rangrim massif is the easternmost part of the Sino-Korean craton; it is a Precambrian terrane consisting of high-grade schists and gneisses, overlain by Mesoproterozoic to Phanerozoic sedimentary rocks and intruded by Mesozoic granitic plutons (Wu et al., 2007a). The massif is dominated by Neoarchean to Paleoproterozoic (2.5–2.6 Ga, 2.1–2.2 Ga, and 1.8–1.9 Ga) magmatic rocks. Zircon Hf isotope data indicate that the continental crust of the Rangrim massif was formed mainly during the Archean and was reworked during the Paleoproterozoic, similar to the eastern North China craton (Wu et al., 2007b). Mesozoic magmatic rocks are widely distributed in the Rangrim massif, including Triassic (224–210 Ma) granite, syenite, dolerite, and kimberlite, as well as Cretaceous (135–110 Ma) granite (Wu et al., 2007a). Cenozoic basalts are also common.

Abundant peridotite xenoliths are found in Late Triassic kimberlites and in Tertiary basalts (Fig. 1). The host kimberlites contain phlogopite that yields an Rb-Sr isochron age of 223.3 ± 6.6 Ma, and the basalts have a whole-rock $^{40}Ar/^{39}Ar$ age of 6.60 ± 0.11 Ma (see the GSA Data Repository[1]). The kimberlites have geochemical features similar to Group II kimberlites of Smith (1983), with high initial $^{87}Sr/^{86}Sr$ (~0.7131) and negative $\varepsilon_{Nd}(t)$ (~–20) and $\varepsilon_{Hf}(t)$ (~–26). They are enriched in large ion lithophile elements (LILEs) and light rare earth elements with $(La/Yb)_{CN}$ ratios of 39.5–41.7, and depleted in high field strength elements, indicating that their parental magmas were derived from small-degree partial melting of ancient lithospheric mantle at depths where garnet was stable.

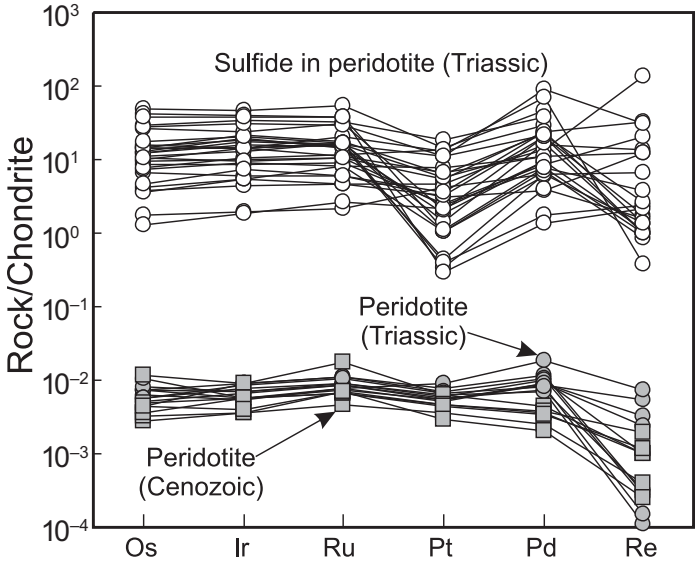

Figure 2. Chondrite-normalized platinum group element (PGE) +Re patterns of peridotite xenoliths and their sulfides from North Korea. PGE and Re data for peridotites were obtained using whole-rock techniques, while those of sulfides were analyzed by laser-ablation–inductively coupled plasma–mass spectrometry.

GEOCHEMICAL FEATURES OF MANTLE XENOLITHS

The mantle xenoliths studied are all spinel peridotites. Xenoliths taken from the kimberlites are generally large (to 30 cm across in largest dimension) and characterized by varying degrees of serpentinization. The xenoliths taken from the Tertiary basalts are small (<5 cm) and fresh, without serpentinization. The peridotites from the Triassic kimberlites and Tertiary basalts have similar mineral compositions. They contain clinopyroxenes and orthopyroxenes with relatively homogeneous CaO and equilibration temperatures of 991–1077 °C for Triassic xenoliths and 904–965 °C for Cenozoic xenoliths (Witt-Eickschen and Seck, 1991). Olivine Mg numbers (%Fo) range from 89 to 91, clinopyroxene Na_2O from 0.46 to 2.10 wt%, and spinel Cr# from 8.8 to 49 (see the Data Repository).

Bulk samples of peridotite xenoliths from the kimberlites and basalts have platinum group element (PGE) + Re concentrations between 0.002 and 0.012 × CI chondrites (Horan et al., 2003), and are all characterized by relatively flat, chondrite-normalized patterns, with the exception of variable Re depletion (Fig. 2). The peridotites in the Triassic kimberlites contain copious sulfides, whereas those in the Cenozoic basalts are characterized by a paucity of sulfides, and those present are generally too small to be analyzed. In situ PGE + Re analyses of sulfides (either enclosed or interstitial) from the peridotites in the Triassic kimberlite have relatively flat chondrite-normalized patterns, like the bulk samples, but with negative platinum anomalies. Platinum depletions in peridotite sulfides have commonly been attributed to exsolution of Pt-Te-Bi rich phases from primary base-metal sulfides during serpentinization (Luguet et al., 2008). There are negative Pt anomalies present in the sulfides, yet the flat whole-rock patterns without Pt depletions suggest that these rocks were not modified by melt-rock interactions that would likely have removed the Pt (Luguet et al., 2008).

The peridotites have whole-rock Os isotope compositions with initial $^{187}Os/^{188}Os$ of 0.1245–0.1295 for those in the Triassic kimberlite, and 0.1218–0.1277 for those in the Tertiary basalt. In situ Os isotope analyses of sulfides in the peridotites from the Triassic kimberlite reveal that the sulfides have variable Os isotopic compositions that largely overlap with the bulk samples, but extend to suprachondritic ratios ($^{187}Os/^{188}Os_i$ = 0.1221–0.1565) (Fig. 3A). Clinopyroxenes in the peridotite from the Triassic kimberlite have relatively unradiogenic Sr ($^{87}Sr/^{86}Sr_i$ = 0.7026–0.7040) and radiogenic Nd [$\varepsilon_{Nd}(t)$ = +6.7 to +13.2] and Hf [$\varepsilon_{Hf}(t)$ = +15.9 to +24.8] isotopic compositions (Fig. 3B).

DISCUSSION

Thermobarometric and isotopic data of the North Korean xenoliths may be combined to determine the thermal and age structure of the lithospheric mantle underlying this region at the time the xenoliths were sampled. The peridotite xenoliths contain no garnet, implying that they probably originated from mantle depths of <~80 km, based on estimates of the spinel-garnet transition in such fertile rocks (Klemme and O'Neill, 2000). Furthermore, the mineral and bulk compositions of the xenoliths suggest that the lithospheric mantle beneath North Korea during the Late Triassic and through the Tertiary was fertile and hot (918–1077 °C). The range and distribution of Os isotope compositions of whole rocks, as well as the Sr-Nd-Hf isotope ratios of the pyroxenes, are within the range of modern convective mantle. The Os isotope compositions of sulfides are also consistent with the range of compositions reported for sulfides present in modern abyssal peridotites (Alard et al., 2005). Collectively, all of these geochemical and isotopic characteristics are consistent with the interpretation that the peridotites represent young (Phanerozoic) additions to the subcontinental lithospheric mantle.

The continental crust of the Rangrim massif was mainly formed during the Archean, and modified by intracrustal fractionation during the Paleoproterozoic (Wu et al., 2007b). Like the Chinese lithospheric mantle to the west, the lithospheric mantle beneath North Korea probably had a similar formation age of at least 2.6–2.5 Ga, and might also have been similarly modified during the Paleoproterozoic (1.9–1.8 Ga) (Gao et al., 2002). From the Mesoproterozoic to Late Permian, North Korea (like the rest of the Sino-Korean craton) was apparently free from magmatic and tectonic activity, and was located some distance from its present position, where it accumulated platform carbonates.

[1]GSA Data Repository item 2010225, methods and supplemental data (figures and tables), is available online at www.geosociety.org/pubs/ft2010.htm, or on request from editing@geosociety.org or Documents Secretary, GSA, P.O. Box 9140, Boulder, CO 80301, USA.

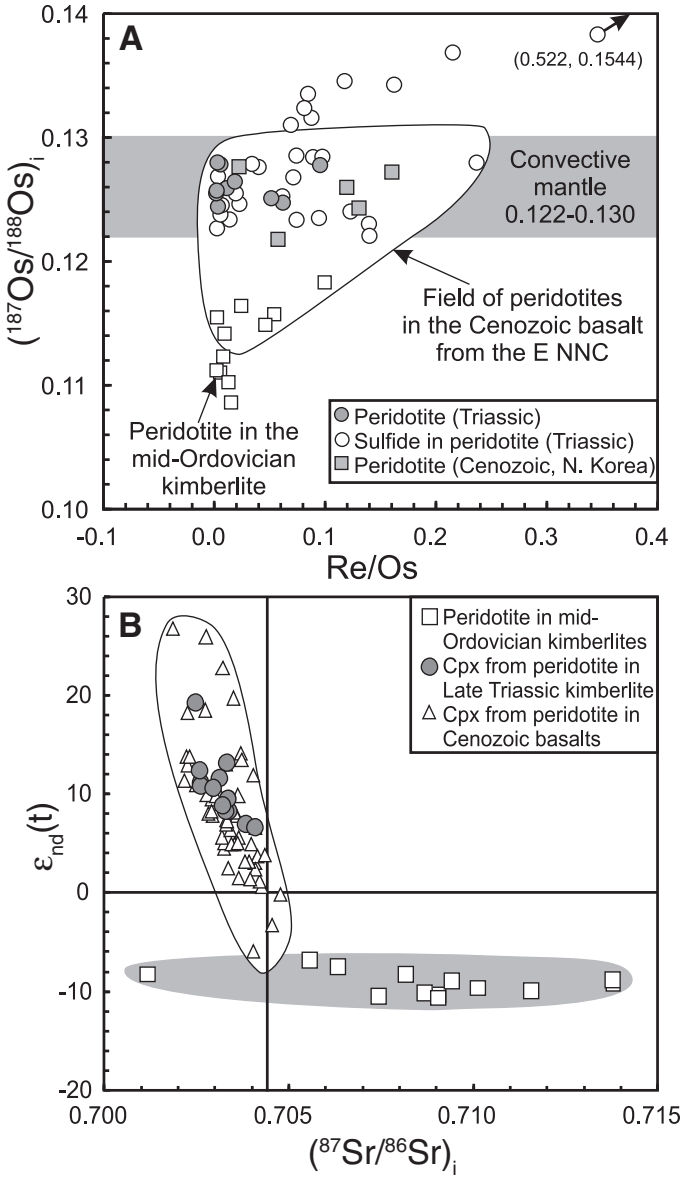

Figure 3. A: Os isotope data for peridotite xenoliths and their sulfides from Late Triassic kimberlites and Cenozoic basalts, compared with those of peridotite xenoliths from Middle Ordovician kimberlites and Cenozoic alkaline basalts in eastern Sino-Korean craton. B: Isotopic compositions of Sr and Nd of clinopyroxenes (cpx) from peridotite xenoliths in Late Triassic kimberlite, compared with those of clinopyroxenes from xenoliths in Middle Ordovician kimberlites and Cenozoic alkaline basalts (from Zheng et al., 2007, and references therein).

The new results for the North Korea xenoliths, coupled with age and mantle source information regarding host volcanics, provide important constraints on the nature and timing of lithospheric replacement under the easternmost portion of the Sino-Korean craton. As with mantle xenoliths present in Mesozoic and Tertiary volcanic rocks in China to the west, the compositional and isotopic data for the subcontinental lithospheric mantle xenoliths present in the Triassic and Tertiary North Korean suites suggest that the ancient lithospheric mantle that presumably underlay this region in the past is no longer present, and was replaced by asthenospheric mantle prior to the Late Triassic. Consequently, the results also provide strong evidence that major lithospheric modification and/or removal affecting the Sino-Korean craton extended eastward to the edge of the craton (North Korea). A key difference between lithospheric replacement under North Korea versus China, however, appears to be timing, which is suggested by several lines of evidence. First, the Chinese basalts that carry the xenoliths with juvenile mantle characteristics have ages of 100 Ma to present (Zheng et al., 2007), whereas the North Korean Triassic kimberlites push the known timing of lithospheric replacement back at least an additional ~120 m.y. Second, the transition of igneous rocks (e.g., basalts) generated from sources with ancient, enriched mantle characteristics to what appears to be juvenile depleted mantle in the eastern portion of the Sino-Korean craton occurred earlier in the east (until 224–210 Ma) (Yang et al., 2007) compared to the west (ca. 165 Ma; Gao et al., 2004) (Fig. 1). From the east to the west in the eastern Sino-Korean craton, the igneous activity occurred from the Triassic (224–210 Ma) in the east (Yang et al., 2007), whereas in the west the activity occurred from the Jurassic (ca. 190 Ma) (Wu et al., 2005). Collectively, these observations suggest that the timing of increased volcanic activity began earlier in the east, compared to the west, and most likely reflects a westward progression of major lithospheric removal. The fact the North Korean Triassic lavas carry the juvenile lithospheric mantle xenoliths suggests that the lithospheric removal underlying North Korea occurred at least 50 m.y. earlier than the lithospheric removal to the west in China. Given these conclusions, it is important to consider what mechanisms could have led to the gradual, westward lithospheric modification and/or replacement by the asthenospheric mantle over a continental-size region, beginning at the eastern edge of this craton.

Removal of subcontinental lithospheric mantle related to major plate tectonic processes can be accomplished by thermal erosion associated with a rising plume head, by extensional thinning of the lithosphere, or by processes related to foundering of lithosphere during thickening (e.g., Menzies et al., 1993; Xu, 2001; Gao et al., 2004; Zheng et al., 2007). The lack of evidence for a plume in the eastern Sino-Korean craton during the Late Triassic argues against the plume erosion model. Geochronological data show that during the Late Permian to Middle Triassic, there was a progressive collision between the Sino-Korean and Yangtze cratons in the south (Okay and Şengör, 1992). The Pacific Ocean plate has been subducted westward beneath the region since at least the Jurassic (Wu et al., 2007c). Given the recent magmatic and tectonic activity in the Sino-Korean craton, it seems likely that the removal of subcontinental lithospheric mantle is related to these events.

The North Korean kimberlite examined here and the Late Triassic (224–210 Ma) magmatism in North Korea and the Chinese Liaodong Peninsula occurred synchronously with or slightly postdated the regional ultrahigh-pressure metamorphic event at 245–226 Ma to the south and, by inference, the continental collision between the Sino-Korean and Yangtze cratons (Liu et al., 2004). Furthermore, the geochemistry and Sr-Nd-Hf isotopic data of the kimberlites indicate that they were derived via small degrees of partial melting of ancient, reenriched refractory lithospheric mantle within the garnet stability field (>80 km). Thus, ancient lithospheric mantle probably underlay the younger hotter mantle sampled by the xenoliths. This is consistent with observations relating to Late Triassic mafic dikes in the Liaodong Peninsula to the west, whereby one group of dikes originated from ancient lithospheric mantle at depths within the garnet stability field (>80 km), yet a second group of dikes originated from juvenile lithospheric mantle generated at depths where spinel was stable (<80 km) (Yang et al., 2007). Therefore, a lithospheric delamination model, i.e., rapid removal of subcontinental lithospheric mantle through lithospheric delamination associated with contractional tectonics, is most compatible with these observations. Rapid removal of the lower lithosphere would have resulted in passive upwelling of asthenospheric mantle to fill the region vacated by subcontinental lithospheric mantle removal; this new fertile material would have cooled from near-adiabatic to near-lithospheric temperatures to form the new lithospheric mantle. Consequently, the extension associated with the rollback of the subducted Pacific plate beneath the eastern Sino-Korean craton since the Jurassic

induced the widespread Jurassic-to-Cretaceous destruction of the eastern Sino-Korean craton (Xu, 2007).

If our model accurately describes lithospheric destruction for the Sino-Korean craton, it raises the intriguing possibility that similar processes could have led to the rapid breakup of other continental blocks.

ACKNOWLEDGMENTS

This work was supported by the National Natural Science Foundation of China (grants 40634019 and 40925007) and by the U.S. National Science Foundation (grants EAR 0635671 and 0911096). This is contribution 634 of the ARC (Australian Research Council) National Key Centre for the GEMOC (Geochemical Evolution and Metallogeny of Continents) (http://www.gemoc.mq.edu.au). Analyses at GEMOC used instrumentation funded by ARC LIEF (Linkage Infrastructure, Equipment and Facilities) and DEST (Department of Education Science and Training) Systematic Infrastructure Grants, Macquarie University.

REFERENCES CITED

Alard, O., Luguet, A., Pearson, N.J., Griffin, W.L., Lorand, J.P., Gannoun, A., Burton, K.W., and O'Reilly, S.Y., 2005, In situ Os isotopes in abyssal peridotites bridge the isotopic gap between MORBs and their source mantle: Nature, v. 436, p. 1005–1008, doi: 10.1038/nature03902.

Boyd, F.R., Pokhilenko, N.P., Pearson, D.G., Mertzman, S.A., Sobolev, N.V., and Finger, L.W., 1997, Composition of the Siberian cratonic mantle: Evidence from Udachnaya peridotite xenoliths: Contributions to Mineralogy and Petrology, v. 128, p. 228–246, doi: 10.1007/s004100050305.

Fan, W.M., Zhang, H.F., Baker, J., Jarvis, K.E., Mason, P.R.D., and Menzies, M.A., 2000, On and off the North China Craton: Where is the Archaean keel?: Journal of Petrology, v. 41, p. 933–950, doi: 10.1093/petrology/41.7.933.

Gao, S., Rudnick, R.L., Carlson, R.W., McDonough, W.F., and Liu, Y.S., 2002, Re-Os evidence for replacement of ancient mantle lithosphere beneath the North China Craton: Earth and Planetary Science Letters, v. 198, p. 307–322, doi: 10.1016/S0012-821X(02)00489-2.

Gao, S., Rudnick, R.L., Yuan, H.L., Liu, X.M., Liu, Y.S., Xu, W.L., Ling, W.L., Ayers, J., Wang, X.C., and Wang, Q.H., 2004, Recycling lower continental crust in the North China craton: Nature, v. 432, p. 892–897, doi: 10.1038/nature03162.

Griffin, W.L., Zhang, A.D., O'Reilly, S.Y., and Ryan, C.G., 1998, Phanerozoic evolution of the lithosphere beneath the Sino-Korean craton, *in* Flower, M.F.J., et al., eds., Mantle dynamics and plate interactions in East Asia: American Geophysical Union Geodynamics Series 27, p. 107–126.

Horan, M.F., Walker, R.J., Morgan, J.W., Grossman, J.N., and Rubin, A.E., 2003, Highly siderophile elements in chondrites: Chemical Geology, v. 196, p. 27–42, doi: 10.1016/S0009-2541(02)00405-9.

Klemme, S., and O'Neill, H.S.C., 2000, The near-solidus transition from garnet lherzolite to spinel lherzolite: Contributions to Mineralogy and Petrology, v. 138, p. 237–248, doi: 10.1007/s004100050560.

Kwon, S., Sajeev, K., Mitra, G., Park, Y., Kim, S.W., and Ryu, I.C., 2009, Evidence for Permian-Triassic collision in far East Asia: The Korean collisional orogen: Earth and Planetary Science Letters, v. 279, p. 340–349, doi: 10.1016/j.epsl.2009.01.016.

Liu, J., Xu, Z., Liou, J.G., and Song, B., 2004, SHRIMP U-Pb ages of ultrahigh-pressure and retrograde metamorphism of gneisses, south-western Sulu terrane, eastern China: Journal of Metamorphic Geology, v. 22, p. 315–326, doi: 10.1111/j.1525-1314.2004.00516.x.

Luguet, A., Pearson, D.G., Nowell, G.M., Coggon, J.A., Dreher, S.T., Spetsius, Z.V., and Parman, S.W., 2008, Enriched Pt-Re-Os isotope systematics in plume lavas explained by metasomatic sulfides: Science, v. 319, p. 453–456, doi: 10.1126/science.1149868.

Menzies, M.A., Fan, W.M., and Zhang, M., 1993, Palaeozoic and Cenozoic lithoprobe and the loss of >120 km of Archean lithosphere, Sino-Korean craton, China, *in* Prichard, H.M., et al., eds., Magmatic processes and plate tectonics: Geological Society of London Special Publication 76, p. 71–81.

Okay, A.I., and Şengör, A.M.C., 1992, Evolution for intracontinental thrust-related exhumation of the ultra-high-pressure rocks in China: Geology, v. 20, p. 411–414, doi: 10.1130/0091-7613(1992)020<0411:EFITRE>2.3.CO;2.

Shirey, S.B., and Walker, R.J., 1998, The Re-Os isotope system in cosmochemistry and high temperature geochemistry: Annual Review of Earth and Planetary Sciences, v. 26, p. 423–500, doi: 10.1146/annurev.earth.26.1.423.

Smith, C.B., 1983, Pb, Sr and Nd isotopic evidence for sources of southern African Cretaceous kimberlites: Nature, v. 304, p. 51–54, doi: 10.1038/304051a0.

Walker, R.J., Carlson, R.W., Shirey, S.B., and Boyd, F.R., 1989, Os, Sr, Nd, and Pb isotope systematics of southern African peridotite xenoliths: Implications for the chemical evolution of subcontinental mantle: Geochimica et Cosmochimica Acta, v. 53, p. 1583–1595, doi: 10.1016/0016-7037(89)90240-8.

Wang, H., and Mo, X., 1996, An outline of the tectonic evolution of China: Episodes, v. 18, p. 6–16.

Witt-Eickschen, G.E., and Seck, H.A., 1991, Solubility of Ca and Al in orthopyroxene from spinel peridotite: An improved version of an empirical geothermometer: Contributions to Mineralogy and Petrology, v. 106, p. 431–439, doi: 10.1007/BF00321986.

Wu, F.Y., Lin, J.Q., Wilde, S.A., Sun, D.Y., and Yang, J.H., 2005, Nature and significance of the Early Cretaceous giant igneous event in eastern China: Earth and Planetary Science Letters, v. 233, p. 103–119, doi: 10.1016/j.epsl.2005.02.019.

Wu, F.Y., Walker, R.J., Yang, Y.H., Yuan, H.L., and Yang, J.H., 2006, The chemical-temporal evolution of lithospheric mantle underlying the North China Craton: Geochimica et Cosmochimica Acta, v. 70, p. 5013–5034, doi: 10.1016/j.gca.2006.07.014.

Wu, F.Y., Han, R.H., Yang, J.H., Wilde, S.A., and Zhai, M.G., 2007a, Initial constraints on the timing of granitic magmatism in North Korea using U-Pb zircon geochronology: Chemical Geology, v. 238, p. 232–248, doi: 10.1016/j.chemgeo.2006.11.012.

Wu, F.Y., Yang, J.H., Wilde, S.A., Liu, X.M., Guo, J.H., and Zhai, M.G., 2007b, Detrital zircon U-Pb and Hf isotopic constraints on the crustal evolution of North Korea: Precambrian Research, v. 159, p. 155–177, doi: 10.1016/j.precamres.2007.06.007.

Wu, F.Y., Yang, J.H., Lo, C.H., Wilde, S.A., Sun, D.Y., and Jahn, B.M., 2007c, The Heilongjiang Group: A Jurassic accretionary complex in the Jiamusi Massif at the western Pacific margin of northeastern China: The Island Arc, v. 16, p. 156–172, doi: 10.1111/j.1440-1738.2007.00564.x.

Xu, Y.G., 2001, Thermo-tectonic destruction of the Archean lithospheric keel beneath eastern China: Evidence, timing and mechanism: Physics and Chemistry of the Earth, part A, v. 26, p. 747–757, doi: 10.1016/S1464-1895(01)00124-7.

Xu, Y.G., 2007, Diachronous lithospheric thinning of the North China Craton and formation of the Daxin'anling-Taihangshan gravity lineament: Lithos, v. 96, p. 281–298, doi: 10.1016/j.lithos.2006.09.013.

Yang, J.H., Sun, J.F., Chen, F.K., Wilde, S.A., and Wu, F.Y., 2007, Sources and petrogenesis of Late Triassic dolerite dikes in the Liaodong Peninsula: Implications for post-collisional lithosphere thinning of the eastern North China Craton: Journal of Petrology, v. 48, p. 1973–1997, doi: 10.1093/petrology/egm046.

Yang, J.H., Wu, F.Y., Wilde, S.A., Belousova, E., and Griffin, W.L., 2008, Mesozoic decratonization of the North China block: Geology, v. 36, p. 467–470, doi: 10.1130/G24518A.1.

Yang, Y.H., Wu, F.Y., Wilde, S.A., Liu, X.M., Zhang, Y.B., Xie, L.W., and Yang, J.H., 2009, In situ perovskite Sr-Nd isotopic constraints on the petrogenesis of the Ordovician Mengyin kimberlites in the North China Craton: Chemical Geology, v. 264, p. 24–42, doi: 10.1016/j.chemgeo.2009.02.011.

Zhao, G.C., Wilde, S.A., Cawood, P.A., and Sun, M., 2001, Archean blocks and their boundaries in the North China craton: Lithological, geochemical, structural and P-T path constraints and tectonic evolution: Precambrian Research, v. 107, p. 45–73, doi: 10.1016/S0301-9268(00)00154-6.

Zheng, J.P., Griffin, W.L., and O'Reilly, S.Y., 2007, Mechanism and timing of lithospheric modification and replacement beneath the eastern North China Craton: Peridotitic xenoliths from the 100 Ma Fuxin basalts and a regional synthesis: Geochimica et Cosmochimica Acta, v. 71, p. 5203–5225, doi: 10.1016/j.gca.2007.07.028.

Manuscript received 7 December 2009
Revised manuscript received 18 March 2010
Manuscript accepted 12 April 2010

Printed in USA

Supplementary information

METHODS SUMMARY

Major elements: Major element analyses of silicate minerals were carried out in the GEMOC Key Centre at Macquarie University using a Cameca SX50 electron microprobe (EMP). The EMP was equipped with five crystal spectrometers, and an accelerating voltage of 15 kV and a sample current of 20 nA were used for the analyses. The width of the electron beam was 5 μm. Standards were well-characterized natural and synthetic materials (e.g. forsterite, chromite, wollastonite, kyanite, albite, rutile, hematite, spessartine, orthoclase, zircon, Y-Al garnet, Hf metal) and matrix corrections were performed following the method of Pouchou and Pichoir (1984). Counting time was 10 s for peaks and 5 s for background on either side of the peak. Accuracy and precision are better than ±0.5 wt.% for major elements.

Clinopyroxene Sr–Nd–Hf isotopes: Strontium, Nd, and Hf isotope compositions of cpx separates from the peridotite xenoliths were determined at the State Key Laboratory of Lithospheric Evolution, Institute of Geology and Geophysics, Chinese Academy of Sciences. The mineral separates were washed with ultra-pure (Milli-Q) water, and ground to 200–400 mesh using an agate mortar before isotopic analysis. About 150–300 mg of cpx powder was weighed into 7 ml SavillexTM Teflon beakers, and appropriate amounts of mixed ^{87}Rb–^{84}Sr, ^{149}Sm–^{150}Nd, ^{176}Lu, and ^{180}Hf spikes were added. Analytical details for sample digestion and column separation procedures are described by Chu et al. (2009).

The Rb–Sr and Sm–Nd isotopic analyses were conducted using a Finnigan MAT 262 thermal ionization mass spectrometer. Measured ^{87}Sr/^{86}Sr and ^{143}Nd/^{144}Nd ratios were corrected for mass-fractionation using ^{86}Sr/^{88}Sr = 0.1194 and ^{146}Nd/^{144}Nd = 0.7219, respectively. During the period of data collection, the measured values for the NBS-987 Sr standard and the JNdi-1 Nd standard were ^{87}Sr/^{86}Sr = 0.710245 ± 16 ($2\sigma_n$, n = 6) and ^{143}Nd/^{14}4Nd = 0.512117 ± 10 ($2\sigma_n$, n = 6), respectively. Lutetium and Hf were measured using a ThermoElectron Neptune multi-collector ICP-MS system. Hafnium isotopic ratios were normalized to ^{179}Hf/^{177}Hf = 0.7325 and ^{176}Lu/^{175}Lu isotopic ratios were normalized using Yb isotopic ratios. During the analytical campaign, an Alfa Hf

standard was measured 10 times and the average value of $^{176}Hf/^{177}Hf$ was 0.282179 ± 4 (2σ).

Whole rock Re–Os and PGE analyses: whole rock Re–Os isotopic compositions and PGE abundances were determined at both the State Key Laboratory of Lithospheric Evolution, Institute of Geology and Geophysics, Chinese Academy of Sciences (IGGCAS) and the Isotope Geochemistry Laboratory, University of Maryland (UMD).

The methods used at both laboratories are similar to those described by Shirey & Walker (1995), and Walker et al. (2008). Rhenium, Os, Ir, Ru, Pt, Pd concentrations and Os isotopic compositions were obtained from the same Carius tube sample digestion (for details of Re–Os and PGE chemistry see Walker et al., 2002, 2008 and Chu et al., 2009).

Osmium isotopic compositions were measured by negative thermal ionization using either a GV Isoprobe-T mass spectrometer at IGGCAS (Chu et al., 2009), or a VG Sector 54 mass spectrometer at UMD (Walker et al., 2002, 2008). For these measurements, purified Os was loaded onto platinum filaments and $Ba(OH)_2$ was used as an ion emitter. At IGGCAS, all samples were run in static mode using Faraday cups. At UMD, samples were run in static mode on Faraday cups, or in peak-jumping mode with a single electron multiplier, depending on the amount of Os. The measured Os isotopic ratios were corrected for mass fractionation using $^{192}Os/^{188}Os = 3.0827$. The in-run precisions for Os isotopic measurements were better than ±0.2% (2RSD) for all the samples. During the period of measurements of our samples, the $^{187}Os/^{188}Os$ ratio of the Johnson–Matthey standard of UMD was 0.11380 ± 4 ($2\sigma_n$, n = 3) at IGGCAS, and 0.11379 ± 2 ($2\sigma_n$, n=3) for Faraday cups and 0.1138 ± 1 ($2\sigma_n$, n = 3) for electron multiplier at UMD.

The isotope dilution analyses of Re, Ir, Ru, Pt, and Pd were conducted either at IGGCAS and UMD using a Thermo-Electron Neptune MC-ICP-MS system with an electron multiplier in peak-jumping mode or using Faraday cups in static mode, according to the measured signal intensity, or at UMD using a Nu-Plasma MC-ICP-MS system with a triple electron multiplier configuration in static mode. Mass fractionations (and gain effects of different multipliers for the UMD method) for Re, Ir, Ru, Pt, and Pd were corrected using Re, Ir, Ru, Pt and Pd standards that were interspersed with the samples. In-run precisions for $^{185}Re/^{187}Re$, $^{191}Ir/^{193}Ir$, $^{194}Pt/^{196}Pt$, $^{105}Pd/^{106}Pd$, and $^{99}Ru/^{101}Ru$ were typically 0.1–0.3% (2RSD).

In-situ Re-Os and PGE analysis of sulfides: The analytical procedures for in situ Re-Os isotopic analysis have been described in detail by Pearson et al. (2002) (also see www.es.mq.edu.

au/GEMOC). Analyses were carrried out using a Merchantek LUV266 laser microprobe with a modified ablation cell, attached to a Nu Plasma multicollector ICPMS. All ablations were carried out using He as the carrier gas, to enhance sensitivity and reduce elemental fractionation. Most analyses were carried out at 4 Hz repetition rate and laser energies of 1–2 mJ/pulse, and typical pit diameters were 50–80 microns. A dry aerosol of Ir, produced by a CETAC MCN6000 desolvating nebuliser, was bled into the gas line between the ablation cell and the ICPMS to provide a mass-bias correction with a precision independent of the abundance of Os in the sample. Masses 188–194 were measured in Faraday cups, and masses 185 and 187 were measured in ETP ion counters. The ion counters were calibrated initially against the Faraday cups and one another using a two-cycle analysis of a standard Os solution, rather than the sequential analysis of Ir + Os and Re + Ir solutions used by Pearson et al. (2002). During ablation runs, a standard NiS bead with 200 ppm Os and Pt (PGE-A) was analyzed between samples, to monitor and correct any drift in the ion counters. These corrections typically were less than 1% over a long day's analytical session. The overlap of ^{187}Re on ^{187}Os was corrected by measuring the ^{185}Re peak and using ^{187}Re/^{185}Re = 1.6741, as described by Pearson et al. (2002). The precision and accuracy of the method are discussed in detail by Pearson et al. (2002). Under ideal circumstances (i.e. sulfides ~50 microns in diameter, and containing at least 40 ppm Os), an internal precision for ^{187}Os/^{188}Os of 0.1–0.3% (2SE) is routinely obtained; for smaller grains or lower Os contents (<5–10 ppm), an internal precision of 1–2% is routine. The external reproducibility of ^{187}Os/^{188}Os for the PGE-A standard over several months is ±0.00048 (2sd), and the mean value of ^{187}Os/^{188}Os is indistinguishable from that derived by TIMS analysis.

In situ PGE analyses were performed with the GEMOC LAM-ICP-MS (Alard et al., 2000). The six PGE, Au, and Se were determined with a custom-built laser ablation system linked to a Perkin-Elmer Sciex ELAN 6000 ICP-MS (RF power, 1050 W). The laser is a Continuum Surelite I-20 Q-switched quadrupled frequency Nd: YAG laser delivering a 266-nm ultraviolet beam. Ablation was done in a pure He atmosphere (0.85L/min). Analytical conditions included a 40- to 60-mm beam diameter, 4 Hz laser frequency, and a beam energy ~0.5 mJ/pulse. Raw data were processed on line by means of the GLITTER software package (Van Achterbergh et al., 1999). ^{63}Cu^{40}Ar interference on ^{103}Rh (monoisotopic) was corrected by ablating a pure Cu metal several times during the run and determining the production rate of ^{63}Cu^{40}Ar. The accuracy of the

correction is checked by correcting ^{105}Pd for $^{65}Cu^{40}Ar$ interference and comparing it to ^{106}Pd, which is free of major interference, except for $^{66}Zn^{40}Ar$. However, Zn abundance in mantle sulfide is generally low <0.3 wt%. A quenched NiS bead doped with PGE and several other chalcophile elements was used as external standard. The similarity of matrix between the standard and the analyzed sulfide allows a straightforward processing of the data (Ballhaus and Sylvester, 2000). The homogeneity of the standard is attested by long-term reproducibility (Alard et al., 2000). Typical detection limit, for the conditions described above, are lower than 40 ppb for all PGE but Ru, which showed a 70 ppb detection limit. Detailed procedure was described by Alard et al. (2000).

References:

Alard, O., Griffin, W. L., Lorand, J. P., Jackson, S. E., O'Reilly, S. Y., Non-chondritic distribution of the highly siderophile elements in mantle sulfides. Nature, 407, 891–894 (2000).

Chu, Z.-Y., Wu, F.-Y., Walker, R. J., Rudnick, R. L., Pitcher, L., Puchtel, I. S., Yang, Y.-H., Wilde, S. A. Temporal Evolution of the Lithospheric Mantle beneath the Eastern North China Craton. Journal of Petrology 50, 1857-1898 (2009).

Pearson, N. J., Alard, O., Griffin, W. L., Jackson, S. E., O'Reilly, S. Y. In situ measurement of Re-Os isotopes in mantle sulfides by laser ablation multi-collector inductively-coupled mass spectrometry: Analytical methods and preliminary results. Geochim. Cosmochim. Acta, 66, 1037–1050 (2002).

Pouchou, J. L., Pichoir, F. A new model for quantitative X-ray microanalysis. Part 1: application to the analysis of homogeneous samples. Rech. Aerosp. 5, 13–38 (1984).

Van Achterberg E., Ryan C. G., Griffin W. L. GLITTER: On line intensity reduction for the laser ablation inductively coupled plasma mass spectrometry. In 9th Goldschmidt Conference, pp. 305. Boston, MA. J. Conf. Abstract, Cambridge, S (1999).

Shirey, S. B., Walker, R. J. Carius tube digestions for low-blank rhenium–osmium analysis. Analytical Chemistry 67, 2136–2141 (1995).

Walker, R. J., McDonough, W. F., Honesto, J., Chabot, N. L., McCoy, T. J., Ash, R. D., Bellucci, J. J. Modeling fractional crystallization of group IVB iron meteorites. Geochimica et Cosmochimica Acta 72, 2198–2216 (2008).

Walker, R. J., Prichard, H. M., Ishiwatari, A., Pimentel, M. The osmium isotopic composition of convecting upper mantle deduced from ophiolite chromites. Geochimica et Cosmochimica Acta 66, 329–345 (2002).

Supplementary data

Table DR1. Rb-Sr isotopic data of phlogopites in the kimberlite from the North Korea

No	Rb [ppm]	Sr [ppm]	$^{87}Rb/^{86}Sr$	$^{87}Sr/^{86}Sr$	2σ
1	72.6	14.6	14.45	0.758565	0.000019
2	30.8	7.56	11.85	0.750505	0.000012
3	31.2	6.02	15.10	0.761392	0.000011
4	22.5	6.02	10.87	0.747459	0.000012
5	37.9	7.59	14.53	0.758846	0.000013
6	19.5	5.11	11.09	0.748270	0.000015
4	20.2	4.43	13.27	0.754990	0.000016

Fig DR1. Rb-Sr isochron age of the phlogopites from the Kimberlite in the North Korea

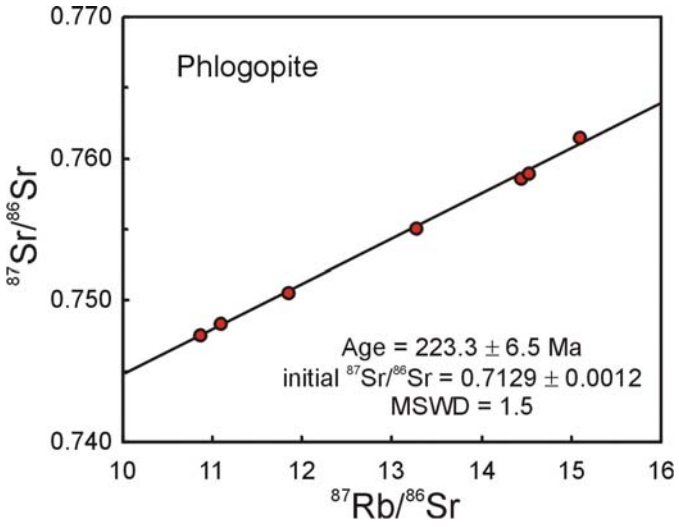

Table DR2. $^{40}Ar/^{39}Ar$ data of whole rock for Cenozoic basalt

t (°C)	^{36}Ar	^{37}Ar	^{38}Ar	^{39}Ar	^{40}Ar	$^{39}Ar/^{40}Ar$	$^{36}Ar/^{40}Ar$	^{39}Ar (%)	Age (Ma)	2 σ
760	0.000046	0.001012	0.000045	0.001302	0.001509	0.08650	0.003045	0.18	13.37	4.75
840	0.000621	0.008471	0.000014	0.031813	0.018254	0.15778	0.003078	4.39	6.63	1.71
880	0.000440	0.006659	0.000014	0.031541	0.016909	0.21465	0.002995	4.35	6.20	1.34
920	0.003363	0.019714	0.000030	0.097440	0.056278	0.09280	0.003203	13.43	6.68	2.85
950	0.000499	0.028109	0.000042	0.114276	0.065208	0.53757	0.002346	15.75	6.59	0.38
980	0.000067	0.027853	0.000030	0.075234	0.042926	1.20069	0.001066	10.37	6.59	0.11
1020	0.000081	0.033481	0.000023	0.050653	0.028988	0.95961	0.001526	6.98	6.61	0.17
1060	0.000150	0.030223	0.000022	0.031419	0.016786	0.51479	0.002453	4.33	6.18	0.45
1100	0.000079	0.031229	0.000020	0.030565	0.017463	0.75174	0.001931	4.21	6.60	0.29

1150	0.000061	0.034676	0.000036	0.033670	0.019175	0.90517	0.001640	4.64	6.58	0.22
1220	0.000169	0.070235	0.000067	0.067539	0.038761	0.76120	0.001906	9.31	6.63	0.25
1300	0.000437	0.753737	0.000171	0.114601	0.067974	0.58103	0.002218	15.80	6.85	0.50
1370	0.000082	0.143441	0.000046	0.020731	0.012254	0.56767	0.002249	2.86	6.83	0.52
1450	0.000146	0.189864	0.000055	0.024558	0.015257	0.42014	0.002501	3.39	7.18	0.84

J = 0.0064030 ± 0.0000160

Plateau Age = 6.60 ± 0.15 Ma, MSWD = 0.65, includes 99.82% of the 39Ar

Isochron Age = 6.60 +/- 0.11 Ma, 40Ar/36Ar = 295.5 +/ 3.7, MSWD = 0.71

Fig DR2. Plateau diagram for the Cenozoic basalt

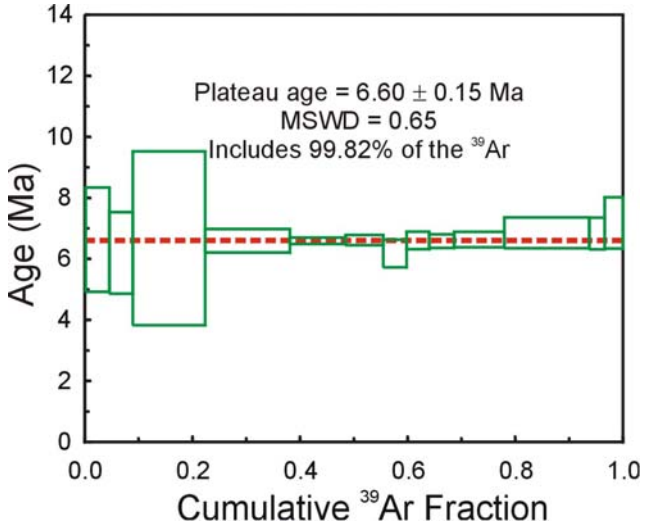

Table DR3. Geochemical and Sr-Nd-Hf isotopic data of Triassic kimberlites from the North Korea

Sample	05NK38	05NK39	Sample	05NK38	05NK39
SiO_2 (wt%)	47.69	45.53	t (Ma)	223	223
TiO_2	0.84	0.88	Rb (ppm)	234	218
Al_2O_3	9.94	9.45	Sr (ppm)	1097	994
TFe_2O_3	8.23	8.73	$^{87}Rb/^{86}Sr$	0.6164	0.6363
MnO	0.10	0.10	$^{87}Sr/^{86}Sr$	0.715121	0.715108
MgO	12.58	12.65	2σ	0.000013	0.000011
CaO	7.54	8.61	$^{87}Sr/^{86}Sr_i$	0.713148	0.713072
Na_2O	1.04	0.44	Sm (ppm)	14.3	14.3
K_2O	4.87	4.35	Nd (ppm)	86.9	86.5
P_2O_5	0.93	0.90	$^{147}Sm/^{144}Nd$	0.0992	0.0998
LOI	5.61	7.67	$^{143}Nd/^{144}Nd$	0.511462	0.511445
TOTAL	99.38	99.31	2σ	0.000013	0.000012
Mg#	75.3	74.3	$\varepsilon_{Nd}(0)$	-22.9	-23.3
Li (ppm)	32	37	$\varepsilon_{Nd}(225)$	-20.2	-20.5
Be	4.3	3.8	$T_{DM}(Nd)$	2126	2158
Sc	18	19	$f_{Sm/Nd}$	-0.50	-0.49
V	113	125	Lu (ppm)	0.22	0.20
Cr	928	1019	Hf (ppm)	4.3	4.6

Co	46	48
Ni	388	424
Cu	43	53
Zn	96	107
Ga	15	15
Rb	230	221
Sr	1041	969
Y	23	25
Zr	219	249
Nb	13	11
Cd	0.036	0.045
Cs	20	28
Ba	3449	3438
La	98.5	105
Ce	193	205
Pr	23.8	25.0
Nd	91.0	93.7
Sm	14.6	15.3
Eu	3.6	3.7
Gd	10.0	10.5
Tb	1.06	1.13
Dy	4.78	5.03
Ho	0.86	0.91
Er	2.01	2.13
Tm	0.28	0.29
Yb	1.79	1.81
Lu	0.25	0.26
Hf	4.95	5.69
Ta	0.65	0.53
Pb	15.2	30.8
Th	16.8	23.5
U	1.99	2.07

$^{176}Lu/^{177}Hf$	0.0071	0.0061
$^{176}Hf/^{177}Hf$	0.281916	0.281904
2σ	0.000008	0.000009
$^{176}Hf/^{177}Hf_i$	0.281886	0.281878
$\varepsilon Hf(t)$	-26.4	-26.7
$T_{DM}(Hf)$	2237	2187
$f_{Lu/Hf}$	-0.79	-0.82

Fig. DR3. Chondrite-normalized REE patterns and Primitive Mantle (PM)-normalized trace element patterns of the kimberlites in the North Korea

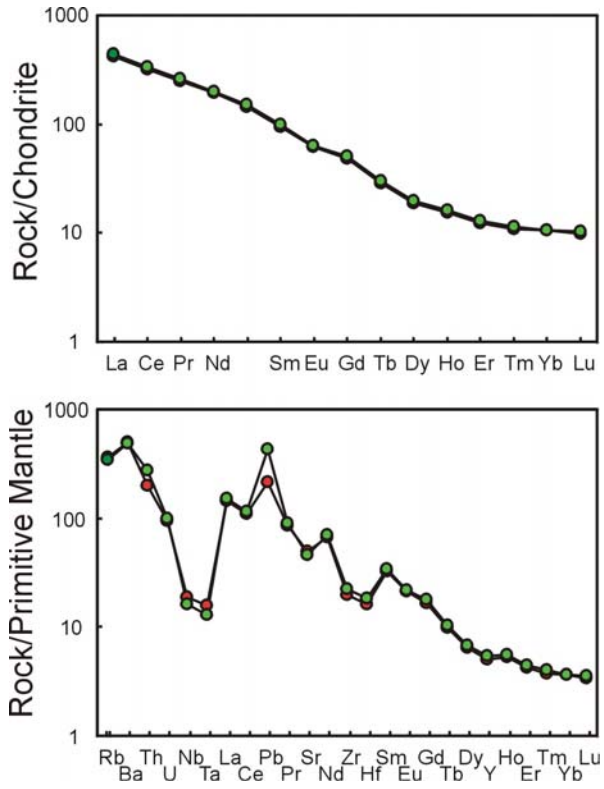

Table DR4. Mineral components of xenoliths in the Triassic kimberlites and Cenozoic basalt from the North Korea

Sample	Min	SiO_2	TiO_2	Al_2O_3	Cr_2O_3	FeO	MnO	MgO	CaO	Na_2O	K_2O	NiO	Total	Fo%	Cr#
05NK41	Ol	41.01	0.00	0.04	0.03	10.66	0.15	48.40	0.09	0.01	0.00	0.38	100.78	89	
05NK42	Ol	41.61	0.00	0.01	0.01	9.08	0.13	49.07	0.04	0.00	0.00	0.41	100.04	91	
05NK43	Ol	41.29	0.00	0.03	0.02	9.94	0.15	49.16	0.08	0.01	0.00	0.40	101.11	90	
05NK44	Ol	41.08	0.00	0.04	0.02	10.43	0.15	48.40	0.10	0.02	0.01	0.39	100.64	89	
05NK45	Ol	40.38	0.00	0.03	0.02	9.94	0.15	48.53	0.08	0.01	0.00	0.37	99.50	90	
05NK46	Ol	41.14	0.01	0.03	0.02	10.32	0.15	48.67	0.08	0.02	0.01	0.39	100.82	89	
05NK47	Ol	41.38	0.01	0.01	0.01	9.20	0.13	48.41	0.06	0.00	0.00		99.22	90	
05NK49	Ol	41.19	0.00	0.03	0.01	10.27	0.15	48.22	0.08	0.02	0.00	0.36	100.34	89	
05NK41	Opx	55.03	0.16	5.16	0.40	6.80	0.15	32.29	0.84	0.15	0.00	0.10	101.07		
05NK42	Opx	55.70	0.08	4.28	0.44	6.02	0.15	33.41	0.66	0.08	0.01	0.10	100.94		
05NK43	Opx	54.69	0.10	5.12	0.47	6.35	0.14	32.32	0.92	0.18	0.01	0.12	100.43		
05NK44	Opx	54.64	0.16	5.52	0.40	6.57	0.14	32.10	1.01	0.18	0.00	0.11	100.84		
05NK45	Opx	54.15	0.15	5.05	0.39	6.33	0.14	32.10	0.89	0.15	0.01	0.11	99.48		
05NK46	Opx	54.70	0.16	5.34	0.39	6.48	0.14	32.19	0.92	0.16	0.01	0.10	100.60		
05NK47	Opx	55.28	0.11	4.84	0.49	6.18	0.14	32.79	0.91	0.13	0.00	0.11	100.98		
05NK48	Opx	54.90	0.14	5.26	0.44	6.34	0.13	32.40	0.91	0.15	0.01	0.10	100.77		
05NK49	Opx	54.49	0.17	5.30	0.39	6.32	0.14	32.25	0.88	0.16	0.00	0.11	100.22		
05NK50	Opx	53.46	0.14	5.39	0.50	6.19	0.14	30.53	1.10	0.15	0.01		97.61		

05NK41	Cpx	51.98	0.63	7.31	0.76	3.38	0.10	15.05	19.11	1.91	0.01	0.05	100.30		
05NK42	Cpx	52.58	0.31	5.96	0.92	2.55	0.09	15.42	20.66	1.56	0.01	0.05	100.10		
05NK43	Cpx	52.21	0.43	7.02	0.93	3.22	0.09	15.55	18.66	1.92	0.01	0.05	100.08		
05NK44	Cpx	51.89	0.57	7.47	0.76	3.38	0.10	15.54	18.63	1.73	0.01	0.05	100.15		
05NK45	Cpx	51.47	0.58	7.08	0.78	3.11	0.10	15.17	19.21	1.72	0.01	0.05	99.29		
05NK46	Cpx	51.91	0.60	7.42	0.74	3.17	0.10	15.41	19.14	1.82	0.01	0.06	100.38		
05NK47	Cpx	52.45	0.39	6.54	0.95	2.97	0.08	15.70	19.68	1.62	0.01	0.05	100.44		
05NK48	Cpx	52.03	0.51	7.05	0.82	3.10	0.08	15.50	19.22	1.72	0.01	0.04	100.09		
05NK49	Cpx	51.70	0.62	7.42	0.77	3.18	0.09	15.34	19.08	1.80	0.01	0.05	100.06		
05NK50	Cpx	51.74	0.48	7.08	0.86	3.60	0.10	15.96	18.65	1.52	0.01	0.05	100.04		
05NK41	Sp	0.10	0.19	56.50	9.59	11.87	0.11	20.05	0.01	0.01	0.00	0.36	98.95		38
05NK42	Sp	0.05	0.09	53.63	13.42	10.59	0.00	20.55	0.01	0.01	0.00	0.38	98.75		49
05NK43	Sp	0.10	0.16	54.44	11.89	11.34	0.13	20.14	0.01	0.00	0.00	0.37	98.71		45
05NK44	Sp	0.09	0.21	56.88	9.89	11.12	0.11	20.32	0.00	0.00	0.00	0.37	99.13		41
05NK45	Sp	0.08	0.18	56.46	9.57	10.89	0.11	20.06	0.00	0.00	0.00	0.34	97.84		40
05NK46	Sp	0.07	0.18	56.63	9.78	10.98	0.12	20.11	0.00	0.00	0.00	0.37	98.38		41
05NK47	Sp	0.06	0.15	53.28	13.79	10.72	0.09	20.62	0.01	0.01	0.01	0.39	98.83		50
05NK48	Sp	0.06	0.16	56.38	10.86	10.34	0.12	20.95	0.00	0.01	0.00		98.89		45
05NK49	Sp	0.09	0.19	57.21	9.33	10.88	0.11	20.43	0.01	0.00	0.00	0.36	98.76		40
05NK50	Sp	0.12	0.23	53.99	12.20	11.50	0.13	20.36	0.00	0.01	0.00	0.34	98.60		45
JB3-1	Ol	41.33	0.01	0.00	0.00	10.47	0.17	48.82	0.02	0.01	0.00	0.39	101.21	89	
JB3-2	Ol	41.88	0.00	0.01	0.01	9.38	0.16	49.74	0.04	0.01	0.01	0.36	101.58	90	
JB3-3	Ol	41.69	0.00	0.00	0.01	9.10	0.13	49.71	0.05	0.01	0.01	0.38	101.09	91	
JB3-4	Ol	41.19	0.00	0.00	0.02	10.33	0.16	48.97	0.03	0.01	0.00	0.39	101.11	89	
JB3-5	Ol	41.56	0.01	0.00	0.00	8.65	0.13	50.30	0.03	0.01	0.00	0.38	101.07	91	
JB3-6	Ol	41.24	0.00	0.00	0.02	8.71	0.15	50.03	0.04	0.00	0.01	0.37	100.59	91	
JB3-1	Opx	55.62	0.10	4.14	0.23	6.52	0.17	32.83	0.49	0.08	0.00	0.10	100.29		
JB3-2	Opx	56.54	0.07	3.62	0.45	5.92	0.14	33.45	0.54	0.07	0.01	0.10	100.89		
JB3-3	Opx	56.60	0.00	3.65	0.45	5.79	0.17	33.56	0.74	0.03	0.00	0.11	101.11		
JB3-4	Opx	56.14	0.10	4.16	0.27	6.52	0.18	33.04	0.49	0.08	0.01	0.13	101.13		
JB3-5	Opx	57.11	0.06	2.44	0.48	5.48	0.16	34.49	0.57	0.04	0.00	0.11	100.96		
JB3-6	Opx	56.90	0.02	2.35	0.46	5.46	0.17	34.20	0.60	0.06	0.00	0.10	100.31		
JB3-1	Cpx	52.81	0.54	7.00	0.69	2.65	0.07	14.38	20.15	2.05	0.00	0.05	100.40		
JB3-2	Cpx	53.73	0.37	5.65	1.16	2.41	0.07	15.23	20.57	1.79	0.01	0.03	101.02		
JB3-3	Cpx	53.69	0.08	3.62	0.66	2.47	0.09	17.06	22.42	0.46	0.00	0.07	100.62		
JB3-4	Cpx	53.33	0.57	6.90	0.65	2.51	0.10	14.42	20.05	2.10	0.01	0.02	100.66		
JB3-5	Cpx	53.74	0.17	3.45	1.28	2.21	0.09	16.31	21.60	1.08	0.01	0.03	99.97		
JB3-6	Cpx	53.56	0.06	3.06	1.06	2.21	0.08	16.60	21.94	1.00	0.01	0.03	99.60		
JB3-1	Sp	0.01	0.06	59.76	8.22	10.32	0.11	20.90	0.00	0.00	0.00	0.40	99.78		8.8
JB3-2	Sp	0.03	0.12	50.00	18.46	11.44	0.12	19.65	0.00	0.01	0.00	0.27	100.10		20
JB3-3	Sp	0.04	0.04	48.89	19.00	11.78	0.15	19.71	0.00	0.01	0.00	0.32	99.93		21
JB3-4	Sp	0.03	0.04	59.33	8.11	10.25	0.14	20.62	0.00	0.00	0.00	0.37	98.92		8.8
JB3-5	Sp	0.03	0.16	36.15	33.57	12.46	0.17	17.66	0.00	0.00	0.00	0.18	100.37		38
JB3-6	Sp	0.04	0.09	34.36	34.63	13.45	0.23	17.05	0.00	0.01	0.01	0.20	100.07		40

Fig. DR4. Comparison of the olivine Mg# of the peridotite xenoliths from mid-Ordovician and Late Triassic kimberlites and Cenozoic alkaline basalts in the east Sino-Korean Craton. Data for xenoliths from Triassic kimberlites and Cenozoic basalts in North Korea are from this work; other data from Zheng et al., 2007 and references therein

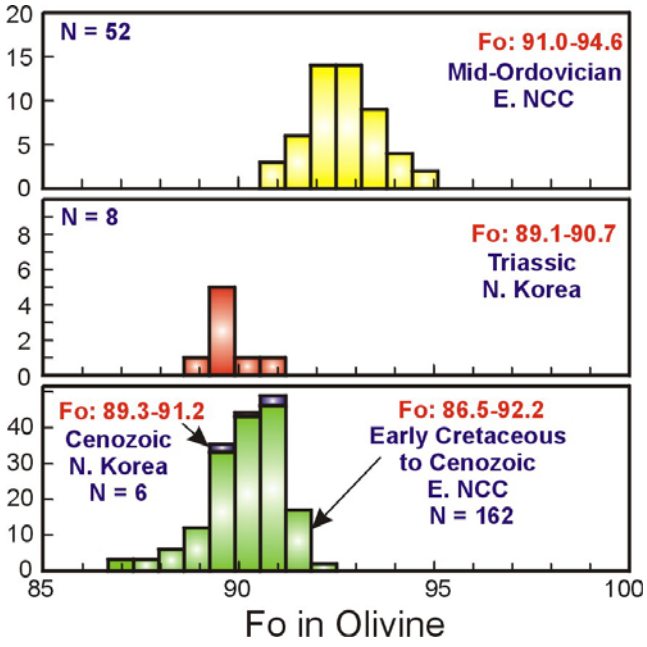

Table DR5. The equilibrium temperatures of the xenoliths in the Triassic kimberlites and Cenozoic basalts from the North Korea

	Temperatures (T °C)			
	[SS81]	[BK Ca in opx @ 15 kBar]	[WES91 - opx-spinel]	[WES91 - Cr-Al-opx]
05NK41	1069	1009	1013	**1010**
05NK42	991	954	958	**991**
05NK43	1076	1034	1041	**1041**
05NK44	1095	1057	1044	**1026**
05NK45	1062	1026	1004	**1009**
05NK46	1081	1031	1027	**1016**
05NK47	1050	1028	1025	**1033**
05NK48	1075	1029	1029	**1033**
05NK49	1073	1023	1015	**1017**
05NK50	1110	1087	1086	**1077**
JB3-1	951	891	880	**904**
JB3-2	947	910	940	**965**
JB3-3	958	978	954	**965**
JB3-4	951	891	879	**918**
JB3-5	899	919	895	**927**
JB3-6	911	932	903	**919**

References*:*

Sachtleben, T., Seck, H. A. Chemical control of Al-solubility in orthopyroxene and its implications on pyroxene geothermometry. Contrib. Mineral. Petrol. 78, 157–165 (1981).

Brey, G.P., Kohler, T. Geothermobarometry in four-phase lherzolites (II): new thermobarometers and practical assessment of existing thermobarometers. J. Petrol. 31, 1353–1378 (1990).

Witt-Eickschen, G. E., Seck, H. A. Solubility of Ca and Al in orthopyroxene from spinel peridotite: an improved version of an empirical geothermometer. Contrib. Mineral. Petrol. 106, 431–439 (1991).

Table DR6. In-situ platinum-group element (PGE) concentrations (ppm) of sulfides in the peridotites from the Triassic kimberlites

No.	Os	Ir	Ru	Pt	Pd	Re
41S01	14.18	21.54	17.62	6.35	23.11	-
41S06	13.14	19.10	14.01	1.84	9.27	-
43S01	9.45	10.20	10.58	5.31	23.80	32.75
43S06	3.71	4.51	4.72	4.63	15.53	13.50
43S07	8.37	8.59	8.87	2.52	8.67	21.00
43S08	6.53	5.93	5.87	3.10	3.85	12.50
43S09	1.80	1.92	2.15	4.21	6.44	6.75
43S10	7.31	8.84	7.99	7.73	11.13	12.50
43S11	12.53	17.38	16.13	10.95	91.31	31.50
45S01	15.04	18.02	15.48	5.67	13.65	135.25
45S02	15.71	14.48	20.73	12.71	28.80	-
45S03	10.12	14.42	10.82	6.63	11.25	-
45S05	4.16	5.38	8.14	1.06	5.91	-
45S06	47.78	47.41	55.27	14.39	47.51	-
45S07	29.27	33.32	32.46	18.91	38.42	--
49S01	0.95	0.80	0.67	0.15	0.74	0.04
49S02	7.82	10.29	11.45	13.73	70.96	0.38
49S03	11.12	12.73	16.89	1.42	16.51	0.98
49S04	26.69	23.47	30.54	2.06	20.53	1.80
49S07	14.49	14.62	16.01	0.33	4.04	1.58
49S07-2	12.24	15.78	15.28	0.44	6.33	1.35
49S08	14.51	13.98	16.73	0.40	1.75	2.35
49S09	17.20	20.62	16.76	1.07	6.85	0.85
49S10	10.65	9.32	10.32	2.40	7.62	1.00
49S12	3.61	5.47	4.65	3.28	20.65	1.00
49S12-2	4.76	7.23	6.11	3.55	23.78	1.38
49S14	42.27	38.95	37.35	0.29	1.37	2.18
49S15	27.96	31.56	29.45	11.02	21.33	2.65
49S15-2	38.69	38.53	37.56	1.12	7.84	3.75

Table DR7. Platinum-group element concentrations and Re-Os isotopic data of peridotites from the Triassic kimberlites (05NK41 to 50) and Cenozoic basalts (JB3-1 to 3-6) in the North Korea

Sample	Rock type	Fo%	Cr%	Re	Os	Ir	Ru	Pt	Pd	$^{187}Re/^{188}Os$	$^{187}Os/^{188}Os$
05 NK 41	**Peridotite**	89	38	0.219	3.542	2.646	5.350	5.467	4.685	0.298	0.12584
05 NK 42	**Peridotite**	90	49	0.012	2.120	4.053	7.971	7.873	6.473	0.026	0.12792
05 NK 43	**Peridotite**	90	45	0.298	3.123	2.485	5.476	9.002	9.909	0.460	0.12946
05 NK 44	**Peridotite**	89	41	0.011	3.658	4.034	8.030	6.916	5.675	0.014	0.12804
05 NK 45	**Peridotite**	90	40	0.127	2.468	3.020	6.055	5.578	4.921	0.248	0.12601
05 NK 46	**Peridotite**	90	41	0.040	3.522	3.222	6.519	6.147	5.503	0.055	0.12612
05 NK 47	**Peridotite**	90	50	0.013	3.922	3.141	6.144	5.824	4.074	0.016	0.12448
05 NK 48	**Peridotite**	-	45	0.004	2.723	3.474	6.573	6.322	3.937	0.008	0.12552
05 NK 49	**Peridotite**	89	40	0.098	5.277	2.607	5.382	5.325	4.917	0.089	0.12677
05 NK 50	**Peridotite**	-	45	0.006	2.842	3.873	7.604	6.662	4.491	0.010	0.12575
JB3-1	**Peridotite**	89	8.8	0.039	5.84	4.193	12.254	6.333	-	0.032	0.12619
JB3-2	**Peridotite**	90	20	0.016	1.34	1.595	3.346	3.551	-	0.057	0.12187
JB3-3	**Peridotite**	91	21	0.040	1.61	1.668	5.091	4.801	-	0.120	0.12603
JB3-4	**Peridotite**	89	8.8	0.078	2.34	2.572	4.823	4.732	-	0.161	0.12723
JB3-5	**Peridotite**	91	38	0.047	1.73	2.564	4.731	4.491	-	0.131	0.12439
JB3-6	**Peridotite**	91	40	0.010	2.18	1.814	4.896	2.906	-	0.023	0.12765

Table DR8. In-situ Re-Os isotopic data of sulfides in the peridotites from the Triassic kimberlites

Sample No	$^{187}Re/^{188}Os$	1σ	$^{187}Os/^{188}Os$	1σ	Initial Os ratio	γOs(t)
05NK41 s02	0.7809	0.0250	0.13713	0.00086	0.13426	7.03
05NK41 s03	0.4216	0.0068	0.13314	0.00032	0.13159	4.83
05NK41 s04	0.0663	0.0013	0.12362	0.00068	0.12338	-1.62
05NK41 s07	2.5138	0.0330	0.16359	0.00089	0.15435	22.98
05NK41bs00	1.1915	0.0180	0.12046	0.00080	0.11608	-7.48
05NK41bs01	0.5975	0.0069	0.11802	0.00091	0.11582	-7.66
05NK41bs07	0.6718	0.0260	0.12550	0.00050	0.12303	-1.92
05NK43 s04	1.1388	0.0160	0.13215	0.00087	0.12797	2.00
05NK43bs09	0.3430	0.0042	0.12805	0.00030	0.12679	1.09
05NK43bs13	0.4290	0.0065	0.12999	0.00072	0.12842	2.38
05NK45 s05	0.5660	0.0046	0.13663	0.00061	0.13455	7.27
05NK45 s09	0.3324	0.0045	0.13224	0.00081	0.13102	4.46
05NK45bs02	0.4544	0.0027	0.12517	0.00044	0.12350	-1.54
05NK45bs04	0.1089	0.0006	0.12504	0.00039	0.12464	-0.62
05NK46 bs01	0.0937	0.0040	0.12584	0.00018	0.12550	0.07
05NK46 bs02	0.0161	0.0010	0.12691	0.00034	0.12685	1.15
05NK46 bs03	0.0121	0.0002	0.12272	0.00022	0.12268	-2.18
05NK46 s05	0.4068	0.0060	0.13502	0.00081	0.13353	6.46
05NK46 s06	0.0267	0.0004	0.12388	0.00025	0.12378	-1.30
05NK46 s07	0.0321	0.0002	0.12466	0.00013	0.12454	-0.69
05NK49 bs00	0.1924	0.0016	0.12832	0.00061	0.12761	1.75
05NK49 bs01	0.2956	0.0037	0.12635	0.00029	0.12526	-0.13
05NK49 bs03	0.1636	0.0065	0.12846	0.00064	0.12786	1.95
05NK49 bs04a	0.5915	0.0041	0.12620	0.00052	0.12403	-0.65

05NK49 bs04b	0.6739	0.0085	0.12453	0.00033	0.12206	-2.70
05NK49 bs07	0.3573	0.0029	0.12466	0.00073	0.12335	-1.65
05NK49 bs08	0.3568	0.0098	0.12985	0.00063	0.12854	2.48
05NK49 bs10	0.4693	0.0085	0.13017	0.00058	0.12845	2.41
05NK49 s05	1.0354	0.0130	0.14066	0.00074	0.13686	9.09
05NK49 s07	0.3903	0.0067	0.13381	0.00090	0.13238	5.54
05NK41 s02	0.7809	0.0250	0.13713	0.00086	0.13426	7.03
05NK41 s03	0.4216	0.0068	0.13314	0.00032	0.13159	4.83
05NK41 s04	0.0663	0.0013	0.12362	0.00068	0.12338	-1.62
05NK41 s07	2.5138	0.0330	0.16359	0.00089	0.15435	22.98

Table DR9. Sr-Nd-Hf isotopic data of the clinopyroxenes in the peridotites from the Triassic kimberlites

Sam. No.	Rb	Sr	$^{87}Rb/^{86}Sr$	$^{87}Sr/^{86}Sr$	2σ	$^{87}Sr/^{86}Sr_i$
05NK41	0.038	119	0.0009	0.703349	0.000015	0.70335
05NK41*			*0.0009*	**0.703289**	**0.000012**	0.70329
05NK42	0.006	31.2	0.0005	0.702455	0.000012	0.70245
05NK43	0.034	121	0.0008	0.703814	0.000013	0.70381
05NK44	0.028	63.3	0.0013	0.702602	0.000013	0.70260
05NK44*				**0.702586**	**0.000023**	
05NK45	0.053	65.4	0.0024	0.703360	0.000013	0.70335
05NK45*			*0.0024*	**0.703336**	**0.000010**	
05NK46	0.031	68.0	0.0013	0.703319	0.000012	0.70331
05NK46*				**0.702579**	**0.000013**	
05NK47	0.082	65.5		0.704074	0.000014	0.70406
05NK48	0.057	90.5	0.0018	0.703185	0.000012	0.70318
05NK48*				**0.703107**	**0.000011**	
05NK49	0.067	69.8	0.0028	0.703115	0.000013	0.70311
05NK49*				**0.703103**	**0.000011**	
05NK50	0.008	60.6	0.0004	0.702944	0.000013	0.70294

Sam. No.	Sm	Nd	$^{147}Sm/^{144}Nd$	$^{143}Nd/^{144}Nd$	2σ	$\varepsilon_{Nd}(0)$	$\varepsilon_{Nd}(225Ma)$	$T_{DM}(Nd)$	$f_{Sm/Nd}$
05NK41	1.28	4.24	0.1829	0.513047	0.000033	8.0	8.4	-4	-0.07
05NK41*	1.79	5.78	0.1877	0.513053	0.000015	8.1	8.4	-3	-0.05
05NK42	0.53	1.24	0.2594	0.513717	0.000021	21.1	19.3	87	0.32
05NK43	1.12	4.76	0.1428	0.512919	0.000018	5.5	7.0	-8	-0.27
05NK44	1.06	2.71	0.2369	0.513269	0.000026	12.3	11.2	7	0.20
05NK44*	1.44	3.71	0.2352	0.513253	0.000017	12.0	10.9	5	0.20
05NK45	1.01	2.38	0.2567	0.513218	0.000093	11.3	9.6	5	0.30
05NK45*	1.22	2.93	0.2520	0.513206	0.000015	11.1	9.5	3	0.28
05NK46	1.05	2.74	0.2310	0.513365	0.000127	14.2	13.2	13	0.17
05NK46*	1.33	3.53	0.2276	0.513321	0.000016	13.3	12.5	8	0.16
05NK47	0.88	2.43	0.2195	0.513013	0.000012	7.3	6.7	-10	0.12
05NK48	1.57	4.27	0.2216	0.513129	0.000015	9.6	8.9	-1	0.13
05NK49	1.73	4.42	0.2373	0.513296	0.000013	12.8	11.7	5	0.21
05NK50	1.03	2.78	0.2236	0.513226	0.000048	11.5	10.7	5	0.14

Sam. No.	Lu	Hf	$^{176}Lu/^{177}Hf$	$^{176}Hf/^{177}Hf$	2σ	$\varepsilon_{Hf}(0)$	$\varepsilon_{Hf}(225Ma)$	$T_{DM}(Hf)$	$f_{Lu/Hf}$
05NK41	0.14	0.88	0.0215	0.283196	0.000007	15.0	16.6	171	-0.35
05NK41*				**0.283174**	**0.000002**				
05NK42	0.11	0.34	0.0468	0.284715	0.000016	68.7	66.6	8590	0.41
05NK42*				**0.284738**	**0.000006**				
05NK43	0.14	0.58	0.0342	0.283377	0.000010	21.4	21.2	-1649	0.03
05NK44	0.16	0.81	0.0282	0.283317	0.000010	19.3	19.9	-354	-0.15
05NK44*				**0.283311**	**0.000003**				

05NK45	0.14	0.64	0.0311	0.283267	0.000010	17.5	17.7	-124	-0.06
05NK45*				**0.283268**	**0.000004**				
05NK46	0.16	0.78	0.0275	0.283325	0.000013	19.6	20.3	-372	-0.17
05NK46*				**0.283321**	**0.000004**				
05NK46*				**0.283314**	**0.000003**				
05NK47	0.12	0.59	0.0287	0.283392	0.000015	21.9	22.5	-785	-0.14
05NK48	0.12	0.69	0.0233	0.283308	0.000011	18.9	20.3	-206	-0.30
05NK48*				**0.283279**	**0.000004**				
05NK49	0.14	0.79	0.0245	0.283267	0.000012	17.5	18.7	-65	-0.26
05NK49*				**0.283248**	**0.000003**				
05NK50	0.09	0.60	0.0217	0.283428	0.000017	23.2	24.8	-574	-0.35

***: duplicate analyses; the bold data are unspiked**

Rb, Sr, Sm, Nd, Lu and Hf (ppm)